# Mean pressure of a finite width oil control ring with randomly spaced grooves

M.-P. Noutary, Nans Biboulet, A.A. Lubrecht

Version of Record: https://www.sciencedirect.com/science/article/pii/S0301679X21001535
Manuscript_b9e95ab91f0300c28807e25b4e1f69cc

# Mean pressure of a finite width Oil Control Ring with randomly spaced grooves

**M.-P. Noutary, N. Biboulet, A.A. Lubrecht***
* ton.lubrecht@insa-lyon.fr
Université de Lyon, INSA-Lyon, LaMCoS, CNRS UMR 5259
Villeurbanne F69621, France

## KEYWORDS

**OCR, surface texture variation, mean pressure**

## ABSTRACT

The current paper studies the pressure generated between two parallel grooved surfaces, as occurs in the oil control ring in internal combustion engines. It is shown that the pressure generated depends significantly on the position of the groove intersections, and thus that a single calculation cannot describe the pressure generated during a full passage of the ring over the pattern. Furthermore, it is shown that the introduction of a groove distance variation reduces the pressure variation, but does not affect the mean pressure generated.

## 1 INTRODUCTION

Internal combustion engine efficiency depends to a large extent on the friction in the Piston Ring Cylinder Liner contact. This contact has been studied numerically for more than four decades, see Dowson et al. [1] and Jeng [2, 3]. More general studies of the piston ring contact can be found in Tian et al. [4], Richardson [5], Gamble et al. [6] and Tomanik [7].

The third ring or the Oil Control Ring (OCR) has the particularity of pressure build-up being mostly dependent on the surface micro-geometry, as its surface is nominally flat and parallel to the liner. Pressure build-up in parallel textured surfaces has been studied by Etsion et al. [8, 9, 10], Tönder [11] and Fowel et al. [12]. The importance of the cavitation pressure was demonstrated by Shen and Khonsari [13, 14, 15] and Ausas et al. [16, 17]. An analysis on textured surfaces in parallel sliders was performed by [18, 19]. Algorithms stressing the importance of mass conservation were developped by Bertocchi et al. [20], Profito et al. [21] and Woloszynski et al. [22]. Optimisation of the textured surface was performed by Codrignani et al. [23]. Chunxing et al. [24] and Wan et al. [25] analysed the interaction of pressure generated by grooves and surface roughness.

To improve the convergence of the mass-conserving algorithm by Woloszynski et al. [22] for very fragmented cavitated domains, a MultiGrid-like extension was implemented by Biboulet and Lubrecht [26]. Noutary [27] studied different aspects of dimples and grooves in parallel surface lubrication, using a classical MultiGrid code.

Many parameters determine the pressure build-up in the OCR-liner contact, including micro texture parameters, such as groove depth, groove width, groove density, groove angle etc. Earlier work [28] has studied the influence of these parameters on friction and film generation. Perfectly periodic patterns were used and each calculation used a single set of groove depth, angle, width and distance. However, in reality these parameters are not deterministically known, but are part of a random distribution.

The current paper studies the influence of the groove pattern regularity in terms of mean pressure and mean pressure variation during crossing using a very robust and efficient Reynolds solver [26]. Therefore, a groove pattern is generated with constant groove depth, width, angle and *average* groove distance. However, the real groove distance contains a random variation which makes the pattern no longer perfectly periodic. The random variation is a uniform distribution within a range maximum of $\pm 20\%$ of the nominal distance. Thus the groove distance varies inside the pattern, but more importantly, the position where the grooves intersect varies. In the rest of this paper, a periodic pattern (hence with no variation in the groove distance) will be designated as *regular*, conversely a non-periodic pattern will be designated as *irregular*.

## 2 EQUATIONS

The hydrodynamic lubrication of the OCR-cylinder liner contact can be described by the Reynolds equation. In order to have a mass conserving algorithm, the following complementary problem is solved:

$$\frac{\partial}{\partial x}\left(\frac{\rho h^3}{12\eta}\frac{\partial p}{\partial x}\right)+\frac{\partial}{\partial y}\left(\frac{\rho h^3}{12\eta}\frac{\partial p}{\partial y}\right)-u_m\frac{\partial(\rho\theta h)}{\partial x}-\frac{\partial(\rho\theta h)}{\partial t}=0 \tag{1}$$

with

$$\begin{aligned} &(p > p_{cav} \quad \text{if} \quad \theta = 1) \\ &(p = p_{cav} \quad \text{if} \quad 0 < \theta < 1) \end{aligned} \tag{2}$$

where $p$ is the hydrodynamic pressure, $h$ the geometry, $u_m$ the mean velocity. The lubricant density $\rho$ and the viscosity $\eta$ are considered constant.

The ring circumference is roughly 20 cm, and its width is 1.2 mm. However, such a large difference in dimensions is not practical from a calculation time point of view because the domain would require a very large number of points in the circumferential direction. Therefore, the calculation domain was chosen as a 24x1.2 mm rectangle, using Dirichlet boundary conditions. For a regular groove pattern, with a zero random distance, the problem can be modeled periodically in the circumferential direction and periodic boundary conditions could have been used there. However, with the random component added to the groove distance, this is no longer possible and Dirichlet conditions are required. These Dirichlet boundary conditions have a significant influence on the pressure distribution close to domain edges at $y = \pm 12$mm. Hence, only the central part of the domain $y = \pm 6$mm is used to compute the mean pressure in order to limit the influence of the Dirichlet boundary conditions. The pressure distribution depends on the exact position of the ring with respect to the groove pattern. Figure 1 shows that the maximum pressure reached in each pattern varies with its location.

Depending on which surface is textured, ring or liner, the problem is respectively steady-state or time dependent. However, considering an irregular pattern *on the ring*, its precise location with respect to the ring edges changes along the circumferential direction. To calculate an average value, one can either use a very large domain along the circumferential direction, or can perform several calculations shifting the pattern along the sliding direction. The latter option is chosen. If the ring is smooth and the pattern is *on the liner*, not studied in this paper, the calculation is transient and a time average can be calculated. In both cases, the mean pressure varies with the texture location. However, this paper is focused on the averaged value. The minimum mean pressure occurs when the groove intersections occur at the inlet edge. In this case the mean inlet height is the smallest, generating the smallest mean pressure, see the analogy with the Rayleigh step bearing in [28]. The steady-state assumption which is used means that one focuses on the central section of the piston stroke. The squeeze (positive or negative) which becomes significant close to the top and bottom dead center is thus neglected here.

For irregular patterns (see figure 1, operating conditions defined in table 1), one of the main conclusions of this work is that the variation amplitude diminishes in comparison with the regular pattern. In order to obtain an accurate estimation of the position-averaged mean pressure for all possible relative pattern positions during crossing, 16 calculations were performed with the flat ring "sliding" (shifting) over the groove pattern. The mean pressure and its standard deviation (among these 16 positions) are given in the following section.

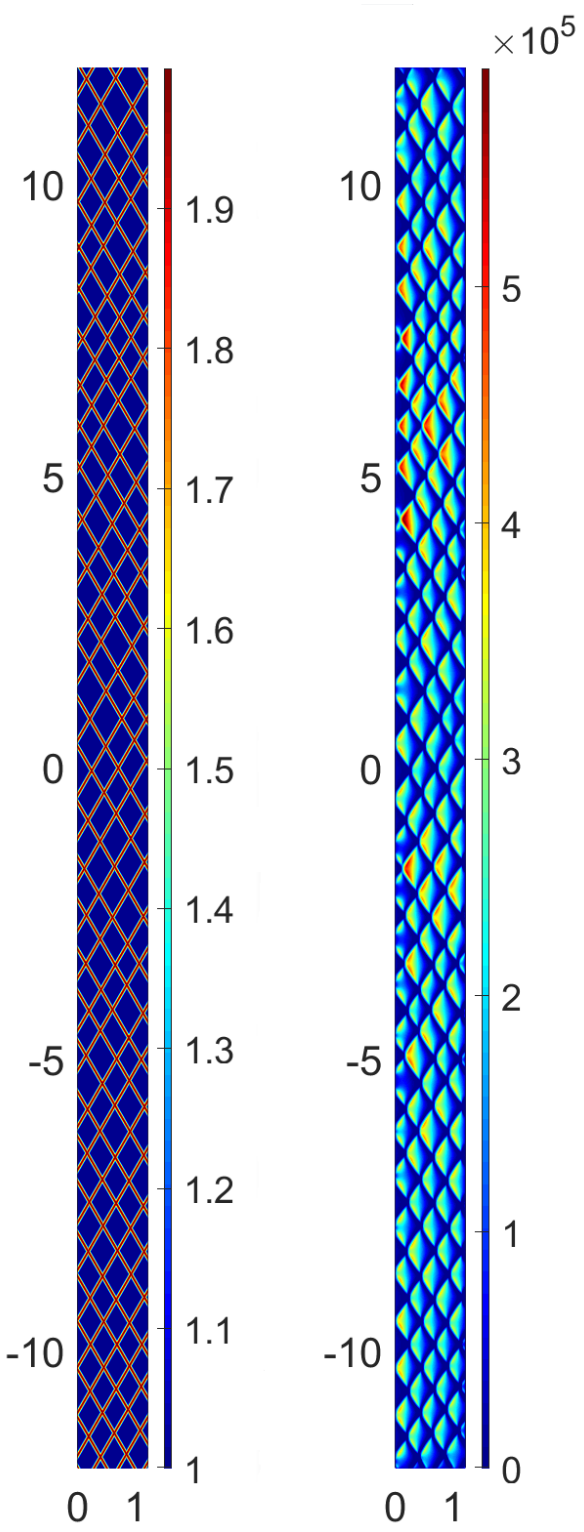


Figure 1: Full calculational domain $x \in [0, 1.2]$ mm, $y \in [-12, 12]$ mm with an irregular groove pattern, geometry (left) geometry colour bar in $\mu$m and pressure (right) pressure colour bar in Pa

## 3 Operating conditions

The operating conditions used throughout the paper are given in table 1, unless otherwise specified, the domain size is $x = 1.2 \times y = 24$ mm, $x$ is in the direction of movement. The groove angle is defined in the appendix fig 11.

| | |
|---|---|
| $\eta_0$ | 0.01 Pa s |
| $u_m$ | 0.5 m/s |
| $p_{amb}$ | 30 kPa |
| angle | 60° |
| groove depth | 1.0 $\mu$m |
| groove width | 0.1 mm |

Table 1: Operating conditions and geometry

The calculations were performed for a fixed minimum film thickness of 1$\mu$m. This choice means that the ring tension is not imposed through a force balance equation; the calculation results in a load carrying capacity expressed as the mean pressure.

# 4 RESULTS

Figure 2 shows the grooves in the central zone (left) and the corresponding generated pressure distribution (right). Please note that scale of the horizontal and vertical axis are different.

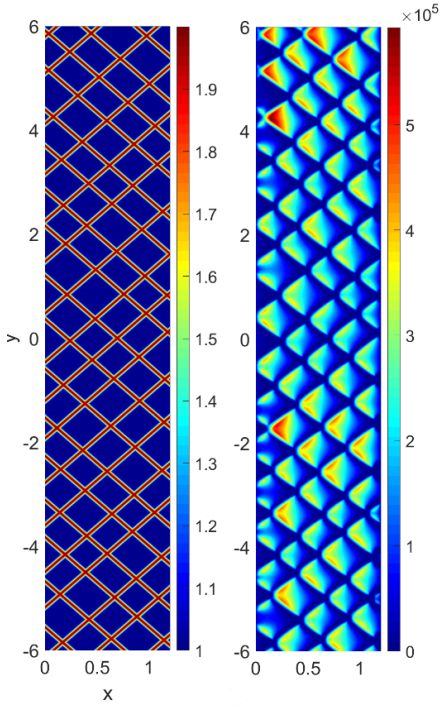


Figure 2: Central part of domain for an irregular pattern, groove geometry (left), pressure (right) ($dist$ = 0.42 mm, $var$ = 20%, geometry colour bar $\mu$m, pressure colour bar in Pa

For a regular groove pattern, all the grooves cross at the same position, hence the mean pressure strongly depends on the exact position of the groove crossings with respect to the ring position. Figure 3 shows the mean pressure for a regular pattern as a function of the relative position between pattern and ring (16 markers). It can be observed that the mean pressure varies roughly by a factor of 4 between the lowest and the highest value. Furthermore, as the pattern is regular, it defines the 16 positions $x_0$ of two full periods. These 16 positions will also be used for irregular patterns, where full periodicity ceases to exist. It will be shown that these 16 positions are sufficient to accurately describe the position averaged mean pressure.

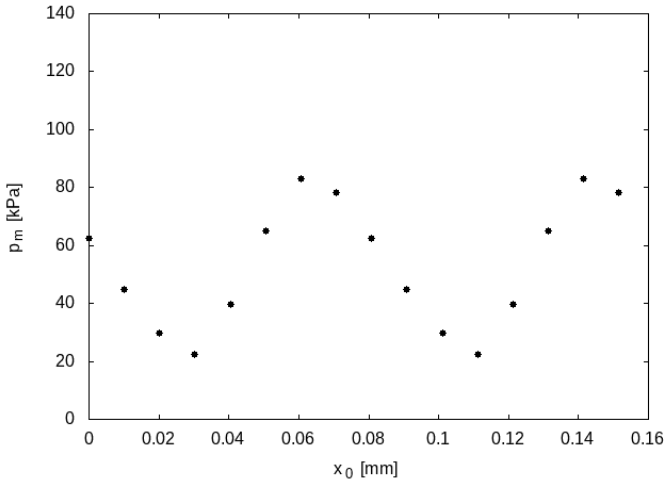


Figure 3: Mean pressure for a regular pattern as a function of the ring position $x_0$ (shift), $dist = 0.14$mm

In order to make the groove pattern more realistic, a relative random component is added to the groove distance, all other groove parameters are fixed. The distance $dist_i$ between groove $i$ and groove $i+1$ is given by the following equation:

$$dist_i = dist \cdot (1.0 + var \cdot rand_i) \tag{3}$$

where one draws from a uniform random distribution $rand_i \in [-1, +1]$, $dist$ is the nominal groove distance (measured perpendicularly to the grooves) and $var$ is the relative distance variation. In this paper, the variations used are: $var = 0.0, 0.05, 0.1, 0.2$. A value of $var = 0.0$ corresponds to a regular pattern. Different seeds are used to obtain different random series.

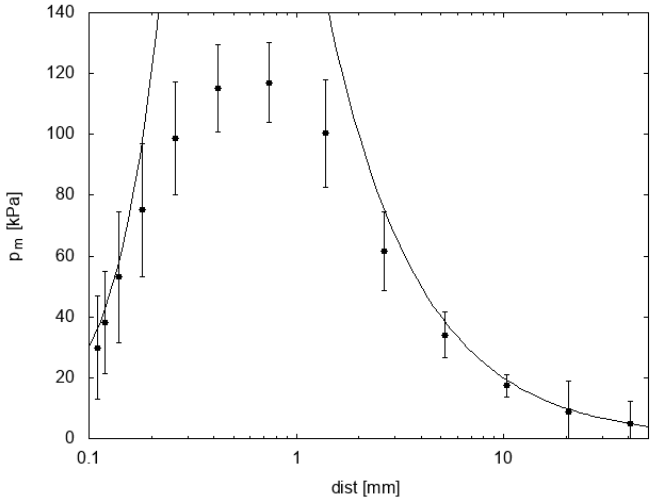


Figure 4: Position-averaged mean pressure (markers) as a function of average groove distance for a regular pattern $var = 0.0$.

Figure 4 shows the position-averaged mean pressure (markers) and its standard deviation among the 16 positions (bars) for a regular pattern as a function of the nominal distance. For small nominal distance values, the position-averaged mean pressure increases with distance, as the small groove distance limits pressure build-up. For a nominal distance of roughly 1 mm, the position-averaged mean pressure reaches a maximum. For even larger nominal distances, the position-averaged mean pressure diminishes. This can seem contradictory to the results from [29] where the mean pressure always increases with the groove distance. In this work the domain covered a complete pattern, therefore as the groove distance increased, the computational domain increased as well. However, in the current work, the physical domain width is limited to 1.2 mm, meaning that when the nominal groove distance increases, fewer grooves are included in the domain.

Thus when the nominal distance increases, parts of the domain do not contain a single groove and therefore the pressure over these parts is close to ambient, see figure 5. For the largest distance used in this work (41), the mean pressure is zero for 6 out of the 16 positions, as there is not a single groove inside the domain. Therefore it is expected that the position-averaged mean pressure is inversely proportional to the groove distance. In order for the reader to approximate the slopes in figure 4, two solid curves are drawn on fig 4: $p_m \propto x^2$ (left) and $p_m \propto 1/x$ (right).

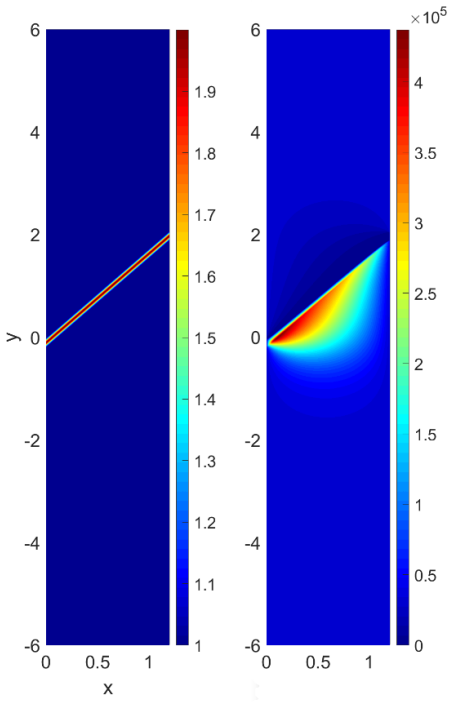


Figure 5: Groove geometry and pressure distribution for a large nominal groove distance of $dist = 10$ and $var = 0.2$, central part of the domain.

Figure 6 shows the mean pressure as a function of the relative position $x_0$ between pattern and ring for $var = 0.1$ (16 positions). Compared with figure 3 where $var = 0.0$, the pressure variation is significantly reduced to $\pm 10\%$. This figure also shows that the mean pressure is no longer perfectly periodic, the second maximum being significantly lower then the first one.

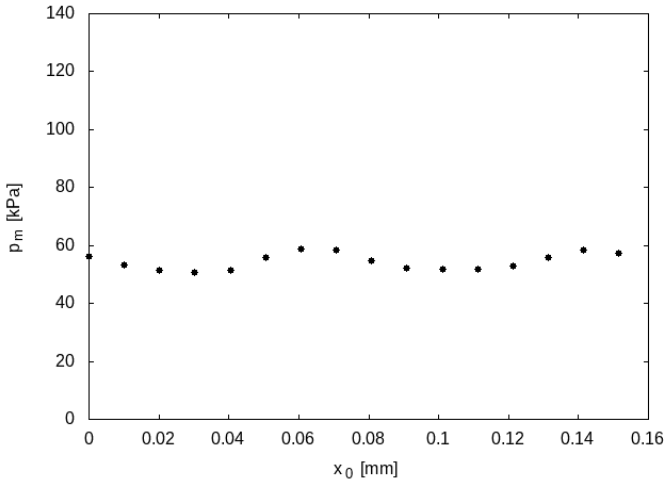


Figure 6: mean pressure as a function of the ring position $x_0$ with respect to the groove pattern $var = 0.1$, $dist = 0.14$mm.

Figure 7 shows the position-averaged mean pressure as a function of the groove distance for a relative distance variation of 10% ($var = 0.1$). The position-averaged mean pressure values are very similar to the ones in figure 4. However, for small nominal distances, the standard deviation (bars) is much smaller, as now the groove distance variations cause the groove intersections to be evenly distributed over the entire domain, including the inlet and outlet. For large nominal distances, the standard deviation increases again, as part of the domain lacks grooves, and its pressure is thus equal to the ambient pressure. For these large groove distances, the standard deviation in the mean pressure is similar to the one in figure 4.

For all calculations, the variations in mean pressure would have been smaller if the domain in the $y$ dimension would have been larger, as one averages over a larger sample. That is why this paper primarily focuses on the position-averaged mean pressure.

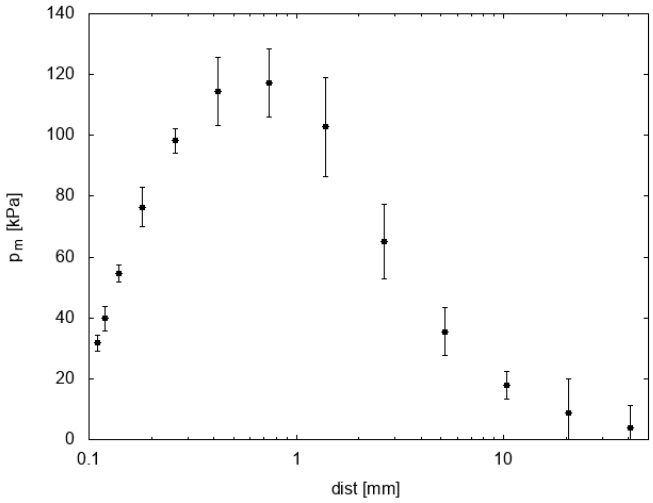


Figure 7: position-averaged mean pressure as a function of average groove distance $var = 0.1$.

Figure 8 shows the results with a 20% variation in the nominal groove distance ($var = 0.2$). The mean pressure and its standard deviation behave in a very similar manner to figure 7 where $var = 0.1$.

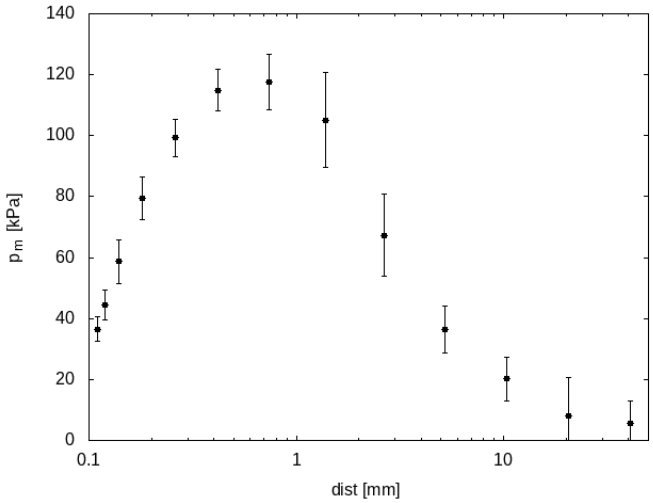


Figure 8: position-averaged mean pressure as a function of average groove distance $var = 0.2$.

In order to validate the accuracy of the trends of the position-averaged mean pressure as a function of the groove mean distance, three different random series were used, and the results are plotted in Figure 9. The differences are minor over the entire distance range, but smallest around $dist = 1$. This means that our samples are sufficiently large to limit the mean pressure variation from one ensemble to another, i.e. the domain size and the value of 16 $x_0$ positions is sufficient.

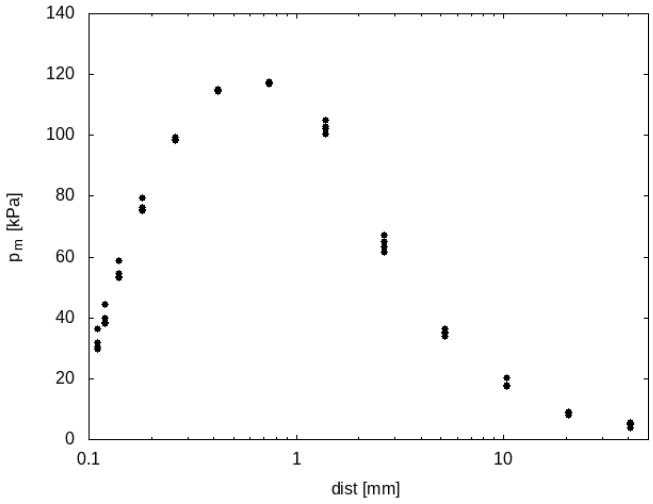


Figure 9: position-averaged mean pressure as a function of average groove distance, for three different series of random numbers, $var = 0.2$.

To complete our understanding of the origins of the position-averaged mean pressure variations as a function of the random distance component, the mean pressures for $var \in [0.0, 0.05, 0.1, 0.2]$ are plotted in Figure 10. For small distances, the variations are minor. For distances between 1 and 10, the variation are a little larger. For $dist \geq 10$ the absolute variations are very small again. A careful observer will only spot 3 dots instead of four. The results for $var = 0$ and $var = 0.05$ differed by less then 2 percent, and the two symbols overlap.

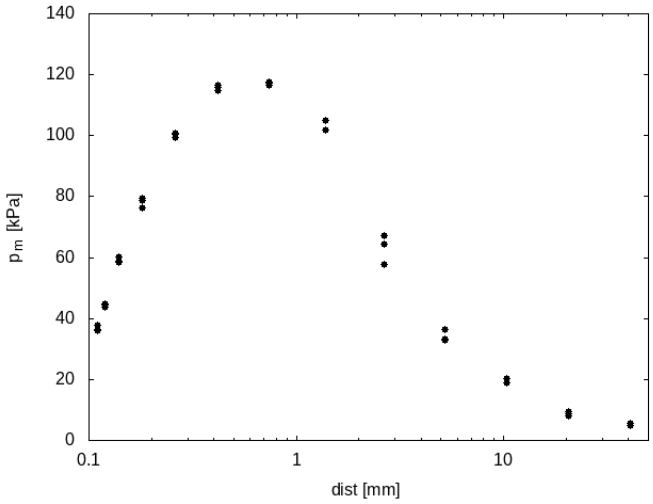


Figure 10: position-averaged mean pressure as a function of average groove distance, $var \in [0.0, 0.05, 0.1, 0.2]$.

The fact the position averaged mean pressure depends very little on the groove distance variation $var$, indicates that the pressure build-up is determined by the local geometry and that the neighbouring geometry plays only a small role. As such averaging the mean pressure will always give a very similar value. Hence the random distance component tends to decrease the mean pressure variation as a function of position, but hardly affects the average mean pressure. Another way to explain this result is that, since the distance variation around the nominal value is limited, one can perform a local linearisation around the nominal value, and patterns with a contribution below average will be compensated by patterns above the average.

As such it is sufficient to study the mean pressure generated by a groove pattern over 16 positions, and knowing that this mean pressure will be very close to that generated by any random distance distribution with the same mean distance.

Typical oil control rings have a smaller land width (0.15 to 0.4 mm) than the 1.2 mm chosen in this study. However, the presented results are useful for an entire range of widths. The implication of a smaller width is that for a given groove distance, the transition from the left to the right part of fig 10 will appear sooner. A smaller size means that a domain without a single groove occurs more rapidly. This transition would occur around the dimensionless groove distance (groove distance over ring width) of 0.8. An other way to see this limit is that the pattern size along the sliding direction must not be much larger than the ring width. The optimum value of the groove distance should be considered relatively to the ring width. If the pattern size is sufficiently small in order to remain on the left part of fig 10, the pressure distribution is well spread on every plateau such as the case illustrated in fig 2. Obviously, this transition is most likely dependent on the groove angle too. Finally, the main conclusions of this study are unchanged: first, the calculation of a single pattern position is not sufficient to judge the performance of a texture, second, the position averaged mean pressure is not modified by a random variation of the groove distance.

# 5 CONCLUSION

The current paper shows the influence of groove distance on the load carrying capacity (mean pressure) for a flat ring (Oil Control Ring). The texture performance can not be predicted based on a single texture location. It was also shown that for small inter groove distances, the mean pressure increases with the inter groove distance. For a distance slightly lower than the ring width, a maximum is reached. For even larger nominal distances the mean pressure diminishes. As the groove pattern has a similar dimension as the ring, the precise position of the ring with respect to the pattern greatly influences the mean pressure built-up. A significant standard deviation for different pattern locations is observed for small distances. When a random variation is added to the groove distance, this large standard deviation decreases for small inter-groove distances. For large inter-groove distances the standard deviation remains large for all cases but this last point is most likely domain size dependent. For these large inter-groove distances, the mean pressure fluctuation is caused by the grooves appearing in the domain or not at all and not by the position of the groove intersections.

Finally, the position-averaged mean pressure depends very little on the variation of the groove distance, hence only the mean groove distance is a significant parameter for pressure generation.

# References


[1] **Dowson D., Economou P.N., Ruddy B.L., Strachan P.J. and Baker A.J.S.**, 1979, "Piston ring lubrication part II: theoretical analysis of a single ring and a complete ring pack", Energy conservation through fluid film lubrication technology: frontiers in research and design. *Proceedings of the ASME winter annual meeting*, p. 23-52.

[2] **Jeng Y.-R.**, 1992, "Theoretical Analysis of Piston-Ring Lubrication Part I - Fully Flooded Lubrication", *STLE Tribology Transactions*, **35**, p. 696-706.

[3] **Jeng Y.-R.**, 1992, "Theoretical Analysis of Piston-Ring Lubrication Part II - Starved Lubrication and the Application to the Complete Ring Pack", *STLE Tribology Transactions*, **35**, p. 707-714.

[4] **Tian T., Wong V.W. and Heywood J.B.**, 1996, "A Piston Ring-Pack Film Thickness and Friction Model for Multigrade Oils and Rough Surfaces", *SAE Paper 962032, SAE Trans., J. Fuels Lubricants*, **105(4)**, p. 1783-1795.

[5] **Richardson D.E.**, 2000, "Review of Power Cylinder Friction for Diesel Engines", *ASME Journal of Eng. for Gas Turbines and Power*, **122**, p. 506-519.

[6] **Gamble R.J., Priest M. and Taylor C.M.**, 2003, "Detailed analysis of oil transport in the piston assembly of a gasoline engine", *Tribol Lett*, **14(2)**, p. 147-156.

[7] **Tomanik E.**, 2013, "Modelling the hydrodynamic support of cylinder bore and piston rings with laser textured surfaces", *Tribology International, Elsevier*, **59**, p. 90-96.

[8] **Etsion I., Kligerman Y., Halperin G.**, 1999, "Analytical and experimental investigation of laser-textured mechanical seal faces", *Tribology Transactions*, **42(3)**, p. 511-516.

[9] **Kligerman Y., Etsion I., Shinkarenko A.**, 2005, "Improving tribological performance of piston rings by partial surface texturing", *Transactions of the ASME, Journal of tribology*, **127**, p. 632-638.

[10] **Etsion I. and Sher E.**, 2009, "Improving fuel efficiency with laser surface textured piston rings", *Tribology International, Elsevier*, **42**, p. 542-547.

[11] **Tonder K.** ,2004, "Hydrodynamics effects of taylored inlet roughness: extended theory", *Tribology International, Elsevier*, **37**, p. 137-142.

[12] **Fowell M. T., Olver A.V., Gosman A.D., Spikes H.A., Pegg I.**, 2007, "Entrainment and inlet suction: two mechanisms of hydrodynamic lubrication in textured bearings", *Transactions of the ASME, Journal of Tribology*, **129**, p. 336-347.

[13] **Shen C., Khonsari M.M.**, 2013, "Effect of dimple's internal structure on hydrodynamic lubrication", *Tribology Letters*, **52**, p. 415-430.

[14] **Shen C., Khonsari M.M.**, 2015, "Numerical optimization of texture shape for parallel surfaces under unidirectional and bidirectional sliding", *Tribology International, Elsevier*, **82**, p. 1-11.

[15] **Shen C., Khonsari M.M.**, 2016, "The effect of laser machined pockets on the lubrication of piston ring prototypes", *Tribology International, Elsevier*, **101**, p. 273-283.

[16] **Ausas R., Ragot P., Leiva J., Jai M., Bayada G., Buscaglia G.**, 2007, "The impact of the cavitation model in the analysis of microtextured lubricated journal bearings.", *Transactions of the ASME, Journal of tribology*, **129**, p. 868-875.

[17] **Ausas R., Jai M., Ciuperca I., Buscaglia G.**, 2013, "Conservative one-dimensional finite volume discretization of a new cavitation model for piston-ring lubrication", *Tribology international, Elsevier*, **57**, p. 54-66.

[18] **Dobrica M.B., Fillon M., Pascovici M.D., Cicone T.**, 2010, "Optimizing surface texture for hydrodynamic lubricated contacts using a mass-conserving numerical approach", *Proceedings of the Institution of Mechanical Engineers, part J: Journal of Engineering Tribology*, **224**, p. 737-750.

[19] **Pascovici M.D., Cicone T., Fillon M., Dobrica M.B.** , 2009, "Analytical investigation of a partially textured parallel slider", *Proceedings of the Institution of Mechanical Engineers, part J: Journal of Engineering Tribology*, **223(2)**, p. 151-158.

[20] **Bertocchi L., Dini D., Giacopini M., Fowell M. T., Baldini A.**, 2013, "Fluid film lubrication in the presence of cavitation: a mass-conserving two-dimensional formulation for compressible, piezoviscous and non-Newtonian fluids", *Tribology International, Elsevier*, **67**, p. 61-71.

[21] **Profito F.J., Giacopini M., Zachariadis D.C., Dini D.**, 2015, "A General Finite Volume Method for the Solution of the Reynolds Lubrication Equation with a Mass-Conserving Cavitation Model", *Tribology Letters*, **60**.

[22] **Woloszynski T., Podsiadlo P., Stachowiak G. W.**, 2015, "Efficient solution to the cavitation problem in hydrodynamic lubrication", *Tribology letters, Springer*, **58(1)**.

[23] **Codrignani A., Savio D., Pastewka L., Frohnapfel B. and van Ostayen R.** 2020, "Optimization of surface textures in hydrodynamic lubrication through the adjoint method", *Tribology International, Elsevier*, **148**

[24] **Chunxing, G., Xianghui, M., Shuwen, W., Xiaohong, D.**, 2020, "Study on the mutual influence of surface roughness and texture features of rough-textured surfaces on the tribological properties", *Proceedings of the Institution of Mechanical Engineers Part J-Journal of Engineering Tribology*, **235**, p.256-273

[25] **Ma, W., Biboulet, N. and Lubrecht A.A.**, 2021, "Cross-hatched groove influence on the load carrying capacity of parallel surfaces with random roughness", *Tribology International, Elsevier*, **153**, p.35-40.

[26] **Biboulet, N. and Lubrecht, A.A.**, 2018, "Efficient solver implementation for Reynolds equation with mass-conserving cavitation", *Tribology International, Elsevier*, **118**, p. 295-300.

[27] **Noutary, M.-P.**, 2017, "A robust Reynolds solver for textured surfaces in the piston-ring cylinder liner contact.", *PhD Thesis*, INSA Lyon.

[28] **Noutary, M.-P., Biboulet, N. and Lubrecht, A.A.**, 2020, "Dimple influence on load carrying capacity of parallel surfaces", *Tribology International, Elsevier*, **149**.

[29] **Biboulet, N., Bouassida, H. and Lubrecht, A.A.**, 2015, "Cross hatched texture influence on the load carrying capacity of oil control rings", *Tribology International, Elsevier*, **82**, p.12-19.

# A Calculation window

In this section, the choice of the calculation window (orange zone in Figure 11) is explained. One regular pattern is considered. The calculation zone is a $24 \times 1.2$ mm band starting in the sliding direction at $x_0$ and ending at $x_1$. The segment $AB$ is decomposed into sixteen equally spaced segments and the point $x_0$ is used to define the 16 positions of the calculation window. The total useful domain in the sliding direction is then the segment $AC$ of total length $d/\sin\alpha + 1.2$ mm where $d$ denotes the nominal distance between grooves and $\alpha$, the groove angle. In Figure 11, only the center line of the grooves is plotted. Of course, when $d$ is much larger than 1.2 mm, as it is the case in the figure, there are only a few grooves inside the calculation zone.

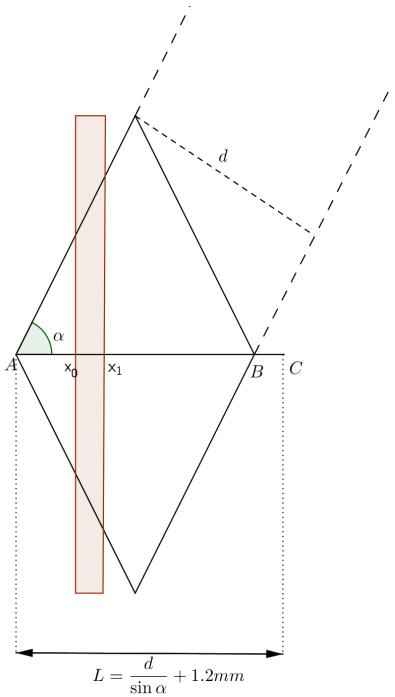


Figure 11: Calculation zone within one pattern.